Assessment of a Data Assimilation Technique for Wind Tunnel Wall Interference Corrections

Belligoli, Zeno; Dwight, Richard; Eitelberg, Georg

DOI
10.2514/6.2019-0939

Publication date
2019

Document Version
Final published version

Published in
AIAA Scitech 2019 Forum

AIAA SciTech Forum
7-11 January 2019, San Diego, California
AIAA Scitech 2019 Forum

10.2514/6.2019-0939

Assessment of a Data Assimilation Technique for Wind Tunnel Wall Interference Corrections

Zeno Belligoli*, Richard Dwight†, and Georg Eitelberg ‡
Faculty of Aerospace Engineering, TU Delft, 2629 HS, Delft, the Netherlands.

Despite a steady decrease in the overall usage of wind tunnels due to the increasing reliability and speed of computational fluid dynamics (CFD), ground testing remains a fundamental part of the development of an air vehicle. In this context, one of the new trends is represented by data assimilation (DA), whereby experimental and numerical measurements are combined together in an attempt to extract more complete and accurate information from the available data. This work presents an assessment of a variational data assimilation framework for the problem of wind tunnel wall interference corrections. The methodology minimizes the discrepancy between experimental measurements and the corresponding values from a Reynolds-averaged Navier-Stokes (RANS) simulation by optimally tuning the free-stream angle of attack and Mach number, as well as a corrective field for the turbulence model. The framework is first validated on synthetic data, and then tested on two cases at high Mach number and low angle of attack using pressure coefficients on the model's surface as the reference measurements. The assimilated pressure coefficients match the reference ones better than those obtained from a linear correction technique. Furthermore, assimilating also a corrective term in the turbulence model improves the quality of the results with respect to assimilating only the angle of attack and Mach number.

I. Introduction

The wind tunnel has been the predominant tool for the development of aeronautical systems for the majority of the twentieth century. However, there has been a steady decline in the overall usage of the wind tunnel in the past three decades [1]. This can be attributed to the shrinking number of aircraft development programs and to the improvements in speed and accuracy of Computational Fluid Dynamics (CFD). As a matter of fact, CFD has become the primary tool for the preliminary design of new air vehicles, and wind tunnel testing is often used for code validation and database building. More specifically, CFD is extensively used to predict the behavior of the aircraft in the attached and mildly separated flow portion of the flight envelope, i.e. the linear regime [2]. Simulations within the linear regime can be easily and quickly carried out with satisfactory accuracy by means of potential-flow codes. In the non-linear regime, e.g. in presence of strong shock waves or large regions of separated flow, the performance of a potential-flow code quickly deteriorates, and even more advanced solvers based on the Reynolds-Averaged Navier-Stokes (RANS) equations fail to capture fundamental flow phenomena due to the assumptions made in the modeling of turbulence. Therefore, in these cases, the bulk of the design work is still done in the wind tunnel. In this regime, however, wind tunnel wall interference usually becomes dominant and obtaining the equivalent free-stream conditions to the in-tunnel measurements becomes challenging [3].

Despite these changes in the operations of the wind tunnel, the scientific community agrees that wind tunnel experiments will not disappear in the future, but will be fused with numerical simulations in order to combine the strengths of both approaches [1, 4, 5]. Indeed, on the one hand, experimental flow measurements offer an accurate representation of the real flow field but are usually contaminated by noise and limited in space or time, on the other hand, numerical simulations provide noise-free information everywhere in the domain, but are dependent on the choice of boundary conditions as well as on the choice of governing equations and turbulence model.

The process of combining experimental and numerical results is known as data assimilation (DA) or data fusion. In data assimilation, one tries to minimize the discrepancy between experimental observations of a quantity of interest (QoI) and the numerical estimation of that same quantity by tuning the inputs of the numerical model such as initial conditions, boundary conditions and/or model parameters. Variational data assimilation does this by means of a gradient-based optimization for which the gradients are obtained in a computationally-efficient way by solving the adjoint equations. DA was first developed in the field of meteorology [6], and has started to be applied to aerodynamic problems in the last ten years.

*PhD Candidate, Department of Aerodynamics, z.belligoli@tudelft.nl
†Associate Professor, Department of Aerodynamics
‡Full Professor, Department of Aerodynamics

One of the most active areas of DA has focused on the correction of RANS modeling uncertainties. In this regards, three main approaches can be identified. The first one, represented by the works of Cheung et al. [7] and Edeling et al. [8, 9], relied on statistical techniques to calibrate the closure coefficients of the turbulence models and managed to effectively address parametric model uncertainties. However, this approach does not take into account the model form uncertainty, thus limiting its scope and generality.

Model form uncertainty was tackled by the work of Duraisamy and co-workers [10–13], whereby a multiplicative term is inserted in one transport equation of the turbulence model as a corrective scalar field. The advantage of this approach lies in that the initial value of the corrective term can be easily set to unity, thus allowing the use of the data assimilation technique at any Reynolds number. A similar approach was pursued by Wang & co-workers [14–16], whereby LES and DNS data were used to assimilate the corrected eddy viscosity field. Despite these advantages, the extent of the correction to the turbulence model is limited by the assumptions made to develop that model. For example, one cannot expect the corrective term to transform a linear eddy viscosity model into one capable of capturing the anisotropy of the Reynolds stress tensor.

Finally, the most general of approaches tries to infer the effect of turbulence as a forcing term to the Navier-Stokes or RANS equations. This method requires no assumptions on the modeling of turbulence, thus allowing for an extremely flexible representation of its effect, not limited by the functional form of the turbulence model. Notable examples in this direction are represented by the work of Foures et al. [17] and Symon et al. [18], where a variational data assimilation framework for low Reynolds number mean flow reconstruction using a vectorial forcing term in the RANS equations as control parameter was developed. A similar control parameter was also adopted by Lemke and Sesterhen [19], who also assimilated the initial and non-reflecting boundary conditions of simple unsteady flows. Mons et al. [20] developed a data assimilation framework for viscous flow at low Reynolds number which was able to tune the unsteady initial and inflow conditions. The applicability of these methods, however, is limited to low Reynolds number flows because of the difficulties encountered in generating a physical base flow solution at higher Reynolds numbers and the likelihood of producing a non-physical forcing term due to the arbitrary form of the model.

Only a few studies addressed the problem of wind-tunnel interference corrections by means of data assimilation. Ma et al. [21] have proposed a variational data assimilation procedure to correct the angle of attack and Mach number of 2D airfoils in the transonic regime. Their results showed that the methodology was able not only to obtain pressure contours that closely matched the experimental ones, but also accurate estimations of the lift and pitching moment coefficients. Their procedure, however, did not take into account the errors associated with the choice of a certain turbulence model which could yield misleading results for the corrected angle of attack and Mach number. This was acknowledged by Kato et al. [22], who proposed a framework, based on the ensemble Kalman filter, with the capability to estimate not only the angle of attack and Mach number, but also other parameters influencing the turbulence model, such as the von Karman constant κ. By doing this, they were able to address the uncertainty associated with the values of (one of) the closure coefficients of the turbulence model, thus providing insights into the variability of the model outputs. Nevertheless, this technique is limited in scope since the functional form of the model is frozen, thus restricting the generality of the methodology. Both approaches combined the experimentally measured surface pressures on a model in a wind-tunnel with CFD calculations without wind tunnel walls, thus directly obtaining the equivalent free-stream conditions which best matched the measured data in a least-squares sense.

This work explores the potential of a variational data assimilation procedure to directly obtain the free-stream conditions that best match the in-tunnel data in a least-squares sense. The methodology can assimilate not only the free-stream angle-of-attack and Mach number, but also a discrepancy term inserted in the transport equation of the turbulence model, thus effectively taking into account the uncertainty associated to the functional form of the turbulence model. First, the DA is tested on synthetic data, and its sensitivity to the quantity and quality of experimental data is assessed. Then, the methodology is applied to experimental data of 2D airfoils at high Mach number and low angle of attack. At the end of this work, the main conclusion of this assessment are summarized as well as some recommendations for the future development of variational data assimilation for wind-tunnel wall interference corrections.

II. Methododlogy

A. The RANS Equations

All the simulations in this study are done using SU2. an open-source CFD suite initially developed by Stanford University [23, 24] and now having several developer groups all over the world. The solver uses the finite volume method (FVM) to solve PDEs on both structured and unstructured grids. As mentioned in the introduction, we focus on test cases that require the correct prediction of turbulence-related phenomena for industrial applications. Our workhorses are the RANS equations, since they are the best compromise between accuracy and computational time

that the industry can afford at the moment. The compressible, steady-state, Navier-Stokes equations with no source term or domain motion can be written in the Eulerian differential form as

$$\begin{cases} \mathcal{R}(\boldsymbol{U}) = \nabla \cdot \boldsymbol{F^c} - \nabla \cdot (\mu_{tot} \boldsymbol{F^v}) = 0 & \text{in } \Omega \\ \boldsymbol{v} = 0 & \text{on } S \\ (W)_+ = W_\infty & \text{on } \Gamma_\infty \end{cases} \tag{1}$$

where

$$U = \begin{Bmatrix} \rho \\ \rho \boldsymbol{v} \\ \rho E \end{Bmatrix}, \qquad \boldsymbol{F^c} = \begin{Bmatrix} \rho \boldsymbol{v} \\ \rho \boldsymbol{v} \otimes \boldsymbol{v} + \bar{\bar{I}} p \\ \rho E \boldsymbol{v} + p \boldsymbol{v} \end{Bmatrix}, \qquad \boldsymbol{F^v} = \begin{Bmatrix} \cdot \\ \boldsymbol{\tau} \\ \boldsymbol{\tau} \cdot \boldsymbol{v} + c_p \nabla T \end{Bmatrix}, \tag{2}$$

ρ is the fluid density, $\boldsymbol{v} = \{v_1, v_2, v_3\}^T$ is the flow speed in a Cartesian system of reference, E is the total energy per unit mass, p is the static pressure, c_p is the specific heat at constant pressure, T is the temperature. The viscous stress tensor can be written in vector notation as

$$\boldsymbol{\tau} = \nabla \boldsymbol{v} + \nabla \boldsymbol{v}^T - \frac{2}{3} \bar{\bar{I}} \nabla \cdot \boldsymbol{v}. \tag{3}$$

Assuming a perfect gas with a ratio of specific heats γ, and gas constants R, the pressure is determined from

$$p = (\gamma - 1)\rho \Big[E - \frac{1}{2} (\boldsymbol{v} \cdot \boldsymbol{v}) \Big], \tag{4}$$

the temperature is given by

$$T = \frac{p}{\rho R}. \tag{5}$$

The second line in the system of equations (1) represents the no-slip condition to be enforced at solid walls S, while the final line represents a general boundary condition for the characteristic variables W at the far-field boundaries, where the fluid state at the boundary is updated using the state at infinity (free-stream conditions) depending on the sign of the eigenvalues.

For turbulent flows, the corresponding RANS equations are obtained after a Favre averaging of the Navier-Stokes equations in (1) and the inclusion of a suitable turbulence model for the extra term represented by the Reynolds stress tensor $\overline{u_i' u_j'}$. The most widespread turbulence models are those relying on the Boussinesq hypothesis [25], according to which the effect of turbulence can be represented as an increased viscosity such that

$$\mu_{tot} = \mu_{dyn} + \mu_t. \tag{6}$$

In order to close the system of equations, the dynamic viscosity μ_{dyn} is assumed to satisfy Sutherland's law [26] as a function of temperature alone, and the turbulent viscosity μ_t is computed via a selected turbulence model; in this study, the Spalart-Allmaras (SA) model is used [27]. The SA model is a one-equation turbulence model for which the turbulent viscosity is computed as

$$\mu_{tur} = \rho \hat{\nu} f_{v1}, \qquad f_{v1} = \frac{\chi^3}{\chi^3 + c_{v1}^3}, \qquad \chi = \frac{\hat{\nu}}{\nu}, \qquad \nu = \frac{\mu_{dyn}}{\rho}. \tag{7}$$

The SA working variable $\hat{\nu}$ is obtained by solving the following transport equation in conjunction with the mean flow equations:

$$\begin{cases} \mathcal{R}_{\hat{\nu}}(\boldsymbol{U}, \hat{\nu}) = \nabla \cdot \tilde{\boldsymbol{F}}^{\boldsymbol{c}} - \nabla \cdot \tilde{\boldsymbol{F}}^{\boldsymbol{v}} - Q = 0 & \text{in } \Omega \\ \hat{\nu} = 0 & \text{on } S \\ \hat{\nu} = \sigma_\infty \hat{\nu} & \text{on } \Gamma_\infty \end{cases} \tag{8}$$

where the convective, viscous, and source terms are given by

$$\nabla \cdot \tilde{\boldsymbol{F}}^{\boldsymbol{c}} = \boldsymbol{v} \hat{\nu}, \qquad \nabla \cdot \tilde{\boldsymbol{F}}^{\boldsymbol{v}} = -\frac{\nu + \hat{\nu}}{\sigma} \nabla \hat{\nu}, \qquad Q = c_{b1} \hat{S} \hat{\nu} - c_{w1} f_w \Big(\frac{\hat{\nu}}{d_S} \Big)^2 + \frac{c_{b2}}{\sigma} |\nabla \hat{\nu}|^2, \tag{9}$$

the production term is defined as $\hat{S} = |\boldsymbol{\omega}| + \frac{\hat{\nu}}{\kappa^2 d_S^2} f_{v2}$, $\boldsymbol{\omega} = \nabla \times \boldsymbol{v}$ is the fluid vorticity, d_S is the distance from a point in the domain to the nearest wall, and $f_{v2} = 1 - \frac{\chi}{1 + \chi f_{v1}}$. The function f_w is computed as $f_w = g \Big[\frac{1 + c_{w3}^6}{g^6 + c_{w3}^6} \Big]$, where $g = r + c_{w2}(r^6 - r)$

and $r = \frac{\hat{\nu}}{\hat{S}\kappa^2 d_S^2}$. Finally, the set of closure constants for the model is given by $\sigma = 2/3$, $c_{b1} = 0.1355$, $c_{b2} = 0.622$, $\kappa = 0.41$, $c_{w1} = \frac{c_{b2}}{\kappa^2} + \frac{1+c_{b2}}{\sigma}$, $c_{w2} = 0.3$, $c_{w3} = 2$, $c_{v1} = 7.1$.
The far-field boundary condition for the turbulent viscosity imposes a fraction of the laminar viscosity at the far-field; $\hat{\nu}$ is set to zero on viscous surfaces, corresponding to the absence of turbulent eddies very near to the wall.

A multiplicative corrective term is introduced in the turbulence model in order to correct the functional form of the model discrepancy. Following Singh & Duraisamy [12], this is done by re-writing the production term in $\mathcal{Q}$ as $\beta\hat{S}(\boldsymbol{x})$ for every mesh point. Note that the standard SA model is easily retrieved by setting $\beta = 1.0$. The use of a multiplicative correction term has a number of advantages with respect to an additive term. First, it is inherently non-dimensional and, second, it has a simple initial value of unity. The corrective term can assume both positive and negative values, thus being able to influence not only the production term but also the destruction term (by creating negative production). Furthermore, embedding the model discrepancy within the governing equations allows some physical constraints to be satisfied, as opposed to e.g. directly assimilating the turbulent viscosity.

B. The Discrete Adjoint Equations

The SU2 code was developed for shape optimization problems, whereby one seeks to minimize a cost function $\mathcal{J}$ with respect to changes in the shape of a solid boundary S. Therefore, the whole SU2 adjoint code has been developed with the aim of deriving these type of sensitivities by means of either continuous or discrete adjoint techniques. On the other hand, we are interested in minimizing $\mathcal{J}$ with respect to changes to non-geometrical parameters such as the angle of attack, the Mach number, and $\boldsymbol{\beta}$, a corrective field with as many elements as the number of mesh points, whose values are located in the entire computational domain, and not only on solid boundaries.
The capability to compute these kind of sensitivities is not implemented in SU2, and suitable modifications to the code must be added. The difficulty of this step is dramatically reduced with the help of the Algorithmic Differentiation (AD) tool incorporated in SU2 [28,29]. This tool allows quickly computing the discrete adjoint sensitivities of the objective function with respect to any type of geometric or non-geometric design variable. The fundamental idea of AD is that, since a computer code is a sequence of simple operations, it is possible to compute the simulation output and its derivative with respect to some parameters simultaneously by applying the chain rule. Consider the semi-discretized form of the RANS equations

$$\frac{d\boldsymbol{U}^n}{d\tau} + R(\boldsymbol{U}^n) = 0 \tag{10}$$

where $\boldsymbol{U}$ is the vector of flow and turbulence model state variables, and τ is a pseudo time step which may be different in each cell when a local time-stepping technique is used. The expression above can be written in the form of a fixed-point iteration $\boldsymbol{U}^n = \mathcal{G}^n(\boldsymbol{U}^n, \boldsymbol{U}^{n-1}, ...)$, where the expression for $\mathcal{G}^n$ depends on the choice of discretization schemes. For a steady problem we can also write $\boldsymbol{U} = \mathcal{G}(\boldsymbol{U})$. The discrete optimization problem can then be posed as:

$$\begin{aligned} &\min_{\boldsymbol{\theta}} \mathcal{J}(\boldsymbol{U}) \\ &s.t.: \quad \boldsymbol{U} = \mathcal{G}(\boldsymbol{U}, \boldsymbol{\beta}) \end{aligned}$$

where $\boldsymbol{\theta}$ is the vector of control parameters. One can use the Lagrangian to transform the above constrained optimization problem into an unconstrained one:

$$\mathcal{L} = \mathcal{J}(\boldsymbol{U}) - \overline{\boldsymbol{U}}^T [U - \mathcal{G}(\boldsymbol{U}, \boldsymbol{\theta})]' \tag{11}$$

where $\overline{\boldsymbol{U}}$ is the adjoint state vector. The first order optimality conditions are given by $\frac{\partial \mathcal{L}}{\partial \overline{\boldsymbol{U}}} = 0$, $\frac{\partial \mathcal{L}}{\partial \boldsymbol{U}} = 0$, and $\frac{\partial \mathcal{L}}{\partial \boldsymbol{\theta}} = 0$. The first condition is automatically satisfied if the flow governing equations are satisfied, the second requires the adjoint equations to be satisfied, while the third provides the gradients of the objective function with respect to the design variables, and it is satisfied at any local optimum.
Thanks to the efficient implementation of AD in the SU2 suite, the adjoint solver can be automatically updated when primal code modifications are made, and one can easily define new objective functions from any state variable, thus greatly reducing the implementation effort required for the development of the data assimilation framework.

C. The Correction Methodology

The variational data assimilation framework assessed in this paper seeks to find the free-stream Mach number and angle of attack providing the best match between an experimentally measured QoI and the same QoI as predicted

by the numerical solver. This allows to find the so-called first-order corrections to the experimental measurements, i.e. the corresponding free-stream M and α that yield the measured quantity of interest. Note that this approach is not limited to QoIs defined on solid walls but can also incorporate volumetric measurements such as PIV data. This idea was pursued with good results by Ma et al. [21]. However, their approach did not take into considerations the errors associated with the modeling of turbulence in the RANS equations. This is taken into consideration in this work by inserting a corrective field $\boldsymbol{\beta}$ in one of the transport equations of the turbulence model. In the present case, $\boldsymbol{\beta}$ is multiplied to the production term $\hat{S}$ in the SA transport equation in order to target the functional form of the model discrepancy. The complete vector of control parameters is therefore given by $\boldsymbol{\theta} = \{\alpha, M, \boldsymbol{\beta}\}$.
The objective of the data assimilation is that of minimizing the discrepancy between experimental data and their numerical equivalent:

$$\min_{\boldsymbol{\theta}} \mathcal{J} = \sum_{i=1}^{N_d} \left[d_{i,ref}(\boldsymbol{x}) - d_{i,cfd}(\boldsymbol{x}) \right]^2 + \lambda \sum_{j=1}^{N_m} \left[1.0 - \beta_j \right]^2 \tag{12}$$

where the second term on the right-hand side is a regularization factor that penalizes departures of $\boldsymbol{\beta}$ from its initial value of unity with a weight λ, and N_d, N_m are the number of target data points and mesh points, respectively. The regularization parameter λ is directly proportional to the variance of the experimental measurements σ^2_{exp}. More details on the choice of λ can be found in [12]. The pseudo-code for the data assimilation is as follows;

1. Start with an initial guess for the vector of control parameters $\boldsymbol{\theta}$,
2. Compute RANS flow solution,
3. Compute adjoint solution,
4. Use gradients to update $\boldsymbol{\theta}$,
5. Return to step 2 until optimization stopping criterion is reached.

The optimum solution is the best CFD representation of the real flow field around the model under consideration, and directly provides the corrected values of the free-stream angle of attack and Mach number by optimally tuning the turbulence model discrepancy term.

However, the optimization problem in (12) requires reconstructing a steady flow field from only limited measurements. This problem is ill-posed and, as such, has infinitely-many solutions. To partially alleviate this burden, the augmented Lagrangian $\mathcal{L}$ enforces the governing model equations over the entire domain, thus restricting the spectrum of possible solutions to those satisfying these physics-based constraints. Furthermore, the presence of the regularization term prevents $\boldsymbol{\beta}$ from attaining values that are too far from its initial state. Despite these positive influences, uniqueness of the converged solution cannot be guaranteed and the assimilated results should always be carefully inspected and critically evaluated.

III. Results - Synthetic Data

Results based on synthetic data are presented to demonstrate how the data assimilation technique described in this paper can be used to correct wind tunnel wall interference. The case considered is that of a 2D NACA 0012 airfoil at an angle of attack $\alpha = 14$ deg, a Mach number $M = 0.30$, and a chord Reynolds number $Re_c = 7 \times 10^6$. The synthetic data were generated with the two-equation Menter's shear stress transport (SST) turbulence model [30], while all the assimilations were conducted with the Spalart-Allmaras (SA) turbulence model [27]. This ensures having a turbulence-model-related discrepancy between the data and the RANS used to reconstruct them which has to be compensated by $\boldsymbol{\beta}$. These differences can be observed in Fig. 1, where the separation areas predicted by the SST and SA turbulence models have different size and shape.

Two vectors of control parameters $\boldsymbol{\theta_1} = \{\alpha, M\}$, and $\boldsymbol{\theta_2} = \{\alpha, M, \boldsymbol{\beta}\}$ were used for the assimilations in order to study the influence of assimilating $\boldsymbol{\beta}$ on the final results. The regularization parameter λ was set to zero, and the optimization was made to stop either after 100 optimization cycles, or when the norm of the gradients dropped below 10^{-5}, thus indicating that the vector of control parameters was close enough to a minimum.

For all the simulations, a second-order Jameson-Schmidt-Turkel (JST) scheme was used for the spatial integration of the convective fluxes. Turbulent variables were convected using a second-order scalar upwind method, and the viscous fluxes were calculated using the corrected average-gradient method. Implicit, local time-stepping was used to converge the problem to the steady-state solution.

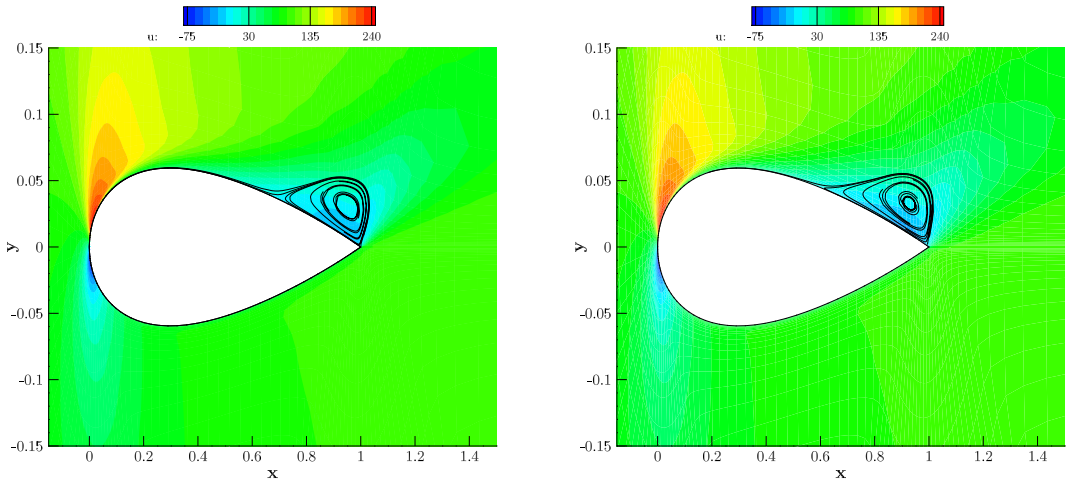

a) SST Model. **b) SA Model.**

Figure 1. Streamwise velocity field for RANS simulations with different turbulence models. The streamlines identify the separation region.

A structured C-grid was used for all simulations. The far-field boundary was placed 500 chord lengths away from the airfoil. A no-slip adiabatic boundary condition was imposed on the airfoil, while characteristics-based boundary conditions were used at the far-field. The minimum cell height in the boundary layer mesh was selected such that $y^+ < 1$. In total, the mesh had 14,336 elements, with 128 edges on the airfoil surface. A close-up of the grid can be seen in Fig. 2.

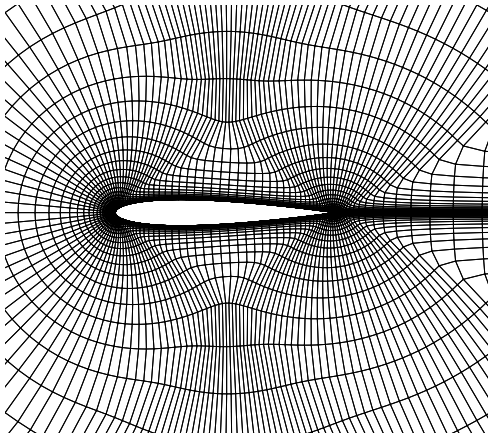

Figure 2. Close-up of the grid for the assimilation with synthetic data.

The pressure coefficient c_p on the surface of the airfoil was selected as the quantity of interest, and a total 128 synthetic measurements were considered. The initial conditions of the data assimilation were $\alpha = 12.5$ deg, $M = 0.27$, and $\boldsymbol{\beta} = \mathbf{1.0}$. The goal was to reconstruct the correct pressure distribution on the airfoil by tuning the angle of attack, Mach number and discrepancy field.

Figure 3 shows the initial and assimilated pressure distributions on the airfoil, and compares them with the reference data, and with a baseline RANS simulation with the SA model and the same angle of attack and Mach number used to generate the synthetic data. The figure shows the assimilated c_p distribution matches the reference better than the initial one. Furthermore, a closer look at the separation region shows the beneficial effect of assimilating the discrepancy term in the turbulence model. The pressure coefficient agrees with the reference data more than the assimilation with $\boldsymbol{\theta}_1$, and both display improvements over the baseline results.

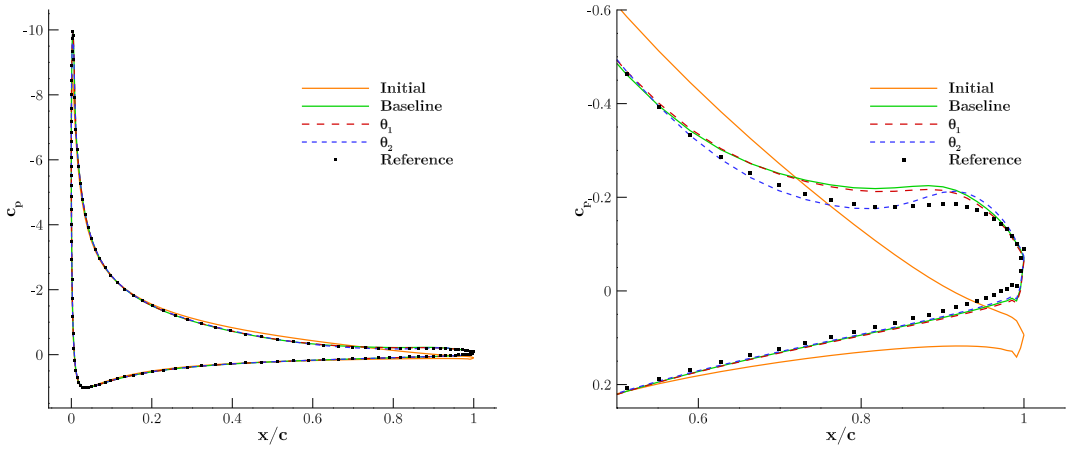

a) Entire airfoil. **b) Trailing-edge region.**

Figure 3. Pressure coefficient over the surface of the airfoil.

Table 1 reports the value of the objective function $\mathcal{J}$ for the data assimilation and the baseline case. We observe that the objective function for the assimilations are approximately 44% and 75% less than that of the baseline, for the cases with $\boldsymbol{\theta}_1$ and $\boldsymbol{\theta}_2$, respectively. Furthermore, while the assimilated Mach number is almost the same as the reference, the assimilated angle of attack is lower. This is because the maximum number of optimization iterations was reached before an optimum solution could be found for $\boldsymbol{\theta}_2$. Nonetheless, the final values of α and M are closer to the reference than those of the assimilation with $\boldsymbol{\theta}_1$, once more proving the advantage of using a corrective term of the turbulence model in the vector of control variables.

	$\mathcal{J}$	α	M	Turb.
Reference	0.0	14.00	0.300	SST
Baseline	5.050×10^{-2}	14.00	0.300	SA
$\boldsymbol{\theta_1}$	2.834×10^{-2}	13.93	0.301	SA
$\boldsymbol{\theta_2}$	1.239×10^{-2}	13.94	0.300	SA

Table 1. Results of the data assimilations with synthetic data. The column with 'Turb.' indicates the kind of turbulence model used.

A. Sensitivity to Available Data

In the preceding example, it has been assumed that pressure measurements are available over the entire airfoil surface. However, in practice, the number of available measurements from an experiment is limited to only a few points on the surface. Hence, it is important to investigate the sensitivity of the reconstructed results to the number of available data. In addition to the assimilation with the full set of 128 data points on the surface of the airfoil, two additional assimilations with 22 and 5 points are conducted. The dataset for the former is obtained by selecting one every six points from the full dataset, whereas the latter only uses 5 points at the leading edge on the upper surface of the airfoil as shown in Fig. 4. Note that all the assimilations were conducted using $\boldsymbol{\theta}_2$ as vector of control variables.

Table 2 reports the results of the data assimilations, all of which are capable of obtaining the correct Mach number, whereas the precision of the assimilated angle of attack decreases with decreasing number of synthetic data points. As observed in the previous section, the angle of attack is the most difficult parameter to correct for this case and therefore its assimilation improves with the number of data available. Yet, it is remarkable that even the assimilated angle of attack with only 5 data points has an error lower than 1% with respect to the reference one.

Figure 5 shows the turbulent viscosity fields for the data assimilations. One can notice that there is no significant difference between the assimilations with the two smallest amounts of available measurements. Both fields display a large turbulent area in the wake of the airfoil, where the flow is separated. On the other hand, in the assimilation with 128 points, this area is much smaller and localized near the trailing edge of the airfoil. This indicates that a smaller

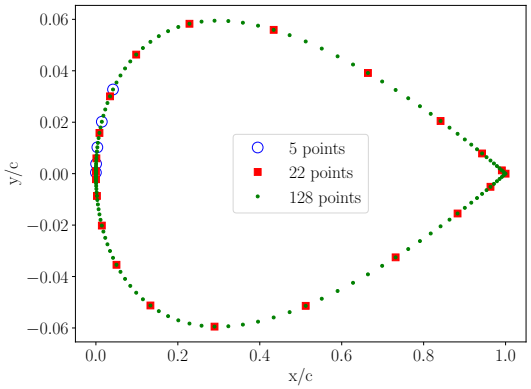

Figure 4. The different locations at which synthetic data were sampled.

# points	$\mathcal{J}$	α [deg]	M	Turb.
128	1.239×10^{-2}	13.94	0.300	SA
22	3.424×10^{-3}	13.91	0.300	SA
5	4.909×10^{-5}	13.87	0.300	SA

Table 2. Results of the assimilations with different amounts of data.

separation bubble is present on the surface of the NACA 0012. These results are also closer to the reference ones, but cannot completely reproduce the stretched shape of the region of high μ_t. This is an indication that the optimization has not converged completely and a larger number of optimization iterations should be taken in the future.

B. Sensitivity to Noise in the Data

In the preceding examples, CFD data have been used to simulate measurements that might be available from an experiment; however, in practice, experimental measurements are contaminated by noise. Therefore the ability of the data assimilation to deal with measurement noise must be addressed. To do this, we modify the synthetic data by adding a random noise component to each c_p measurement as

$$\boldsymbol{d}^* = \boldsymbol{d} + \eta\boldsymbol{\varepsilon}, \tag{13}$$

with $\boldsymbol{\varepsilon}$ a random vector with N_d elements, and η a real number controlling the level of added noise. The vector $\boldsymbol{\varepsilon}$ is constructed by sampling a uniform distribution such that $|\varepsilon_i| < \sqrt{\sum_{i=1}^{N_d} d_i^2 / N_d}$. The level of noise is governed by η; for example, $\eta = 0.1$ corresponds to a noise-to-signal ratio of 10%. In this study, four cases corresponding to noise-to-signal ratios of 1, 5, 10, 25% are investigated. The value of λ is set to zero for all the assimilations in this section in order to be able to compare them. The synthetic data used for the assimilation are the values of the pressure coefficient at all points on the airfoil surface.

Table 3 shows the results of the sensitivity analysis. As expected, the assimilated results deteriorate with increasing level of noise. However, the error in both the angle of attack and Mach number stays below 1% for $\eta \leq 0.1$. Surprisingly, for the assimilation with the highest level of noise, the error in α is kept below 5.2%, while that in M is below 1.3%. These results show the capability of data assimilation to cope with high level of noise in the data, returning reliable estimates for the corrected angle of attack and Mach number.

One additional benefit of this technique is that it can be used to de-noise the measurements taken during a wind tunnel experiment. This can be seen in Fig. 6, where the assimilated pressure coefficients from noisy data are completely smooth. In the same image one can see how the noise level affects the assimilated results: a 5% noise-to-signal ratio already radically changes the pressure distribution at the trailing edge. While this is not affecting the quality of the correction to α and M, it will have a greater effect on the predicted force coefficients and should be object of further investigation.

Figure 7 shows the assimilated turbulent viscosities μ_t for different noise levels. For the cases with the highest levels of noise, the production of turbulence is not enough to reach the high μ_t levels observed in the wake of the airfoil

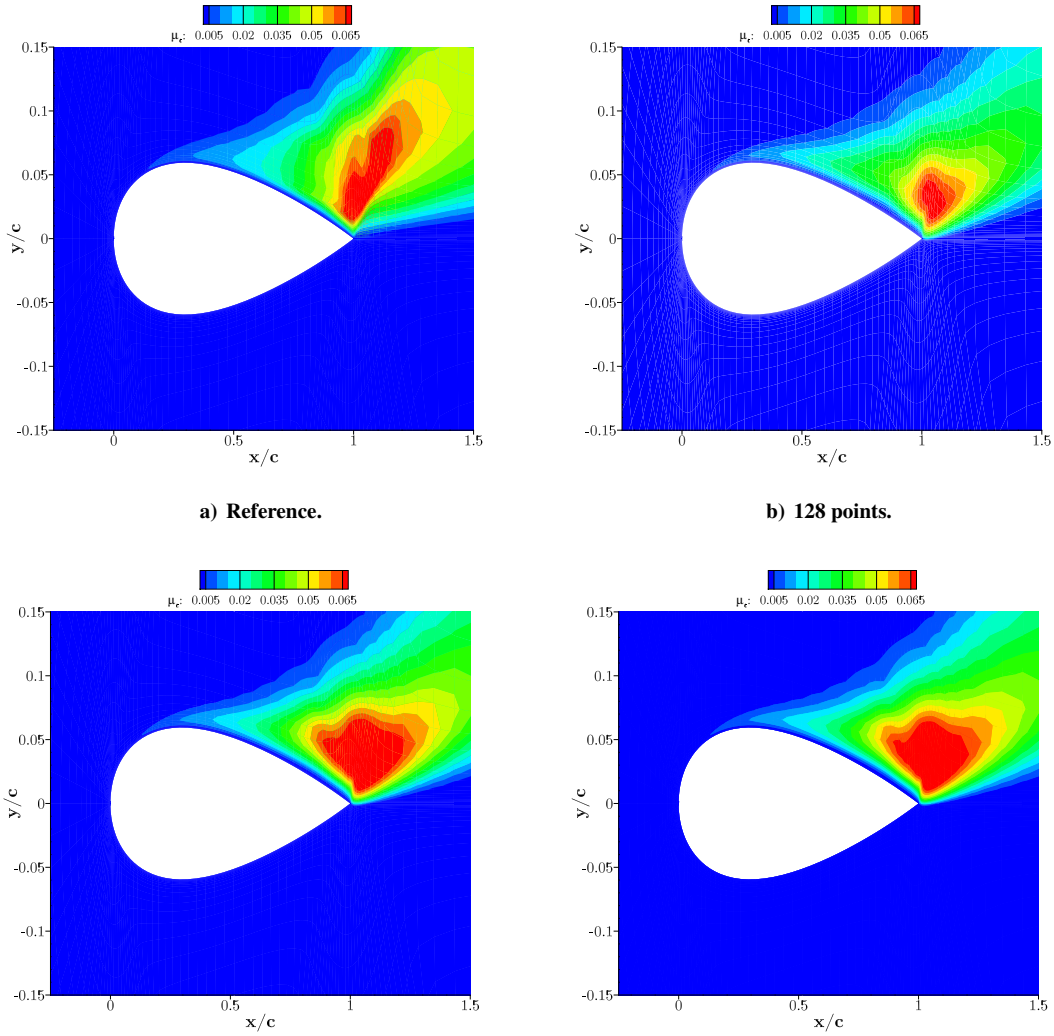

a) Reference. **b) 128 points.**

c) 22 points. **d) 5 points.**

Figure 5. Turbulent viscosity fields for data assimilations with different available synthetic measurements.

η	$\mathcal{J}$	α [deg]	M	Turb.
0.01	4.765×10^{-2}	13.89	0.300	SA
0.05	1.354	14.10	0.302	SA
0.10	4.605	13.89	0.302	SA
0.25	31.23	13.26	0.296	SA

Table 3. Results of the assimilations with different noise levels.

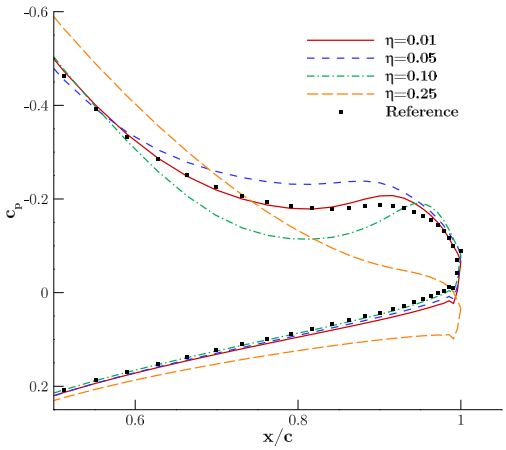

Figure 6. c_p distribution at the final part of the airfoil for assimilations using different noise levels in the data.

for the reference data. The turbulent viscosity field for the assimilation with a 5% noise-to-signal ratio resembles those obtained from assimilations with limited amounts of data in the previous section. This is expected, since both adding noise and removing data points reduce the amount of information available for the data assimilation. Finally, the assimilation with the lowest level of noise produces a μ_t field that is very similar to the one of the noiseless case observed in Section A.

IV. Results - Experimental Data

In this section, a data assimilation of the pressure coefficients obtained from experiments on the RAE 2822 airfoil is conducted with the aim of assessing to what extent DA can be used for the correction of wind tunnel wall interference. The data refer to the experiments conducted by Cook et al. in 1979 [31] which have become widely used for the validation of CFD codes. In this study, we attempt to correct the Mach number and angle of attack for case 6 and case 10, which are a weakly non-linear and a mildly non-linear cases, respectively. Note that by 'non-linear' we intend the deviation of the flow from linear potential theory.

The same hybrid O-mesh geometry was used for both test cases. The far-field boundary was placed 100 chord lengths away from the airfoil to avoid reflections of characteristic waves into the domain. A no-slip adiabatic boundary condition was imposed on the airfoil, while characteristic-based boundary conditions were imposed at the far-field. A layer of structured cells was wrapped around the airfoil, while the rest of the domain was filled with triangular cells. The minimum cell height in the boundary layer mesh was selected such that $y^+ < 3$ for the case with the highest Reynolds number (case 6). In total, the mesh had 22,842 elements, with 192 edges on the airfoil surface.
All the assimilations were performed with a value of $\lambda = 2.6 \times 10^{-3}$, which was chosen in accordance with the accuracy of the pressure measurements on the airfoil surface measured during the experiments. Just as in section III, assimilations with vectors of control parameters identified by $\boldsymbol{\theta}_1$ and $\boldsymbol{\theta}_2$ were conducted for each case.

A. RAE 2822 - Case 6

The initial condition for both the data assimilations with vector of control parameters identified by $\boldsymbol{\theta_1}$ and $\boldsymbol{\theta_2}$ corresponded to the values of Mach number and angle of attack obtained with a linear correction method, i.e. $M = 0.729$, $\alpha = 2.31$ deg. The initial value of $\boldsymbol{\beta}$ was set to unity everywhere in the domain.
Figure 8c shows the optimization history for the two data assimilations. Both assimilations are capable of reducing by approximately 30% the value of the objective function compared to the initial state. Furthermore, the data assimilation with $\boldsymbol{\theta_2}$ is able to reduce the objective function value more than the assimilation with $\boldsymbol{\theta_1}$ thanks to the action of $\boldsymbol{\beta}$, which effectively corrects the small inadequacies in the turbulence model. Note that the sudden peaks in the objective function values arise naturally due to the line search algorithm failing to find an appropriate step size for that particular iteration.

Figures 8a and 8b show the comparison of the pressure-coefficient distribution over the airfoil among the different data assimilations and the reference data. Almost no difference is observed between the results of the two assimilations

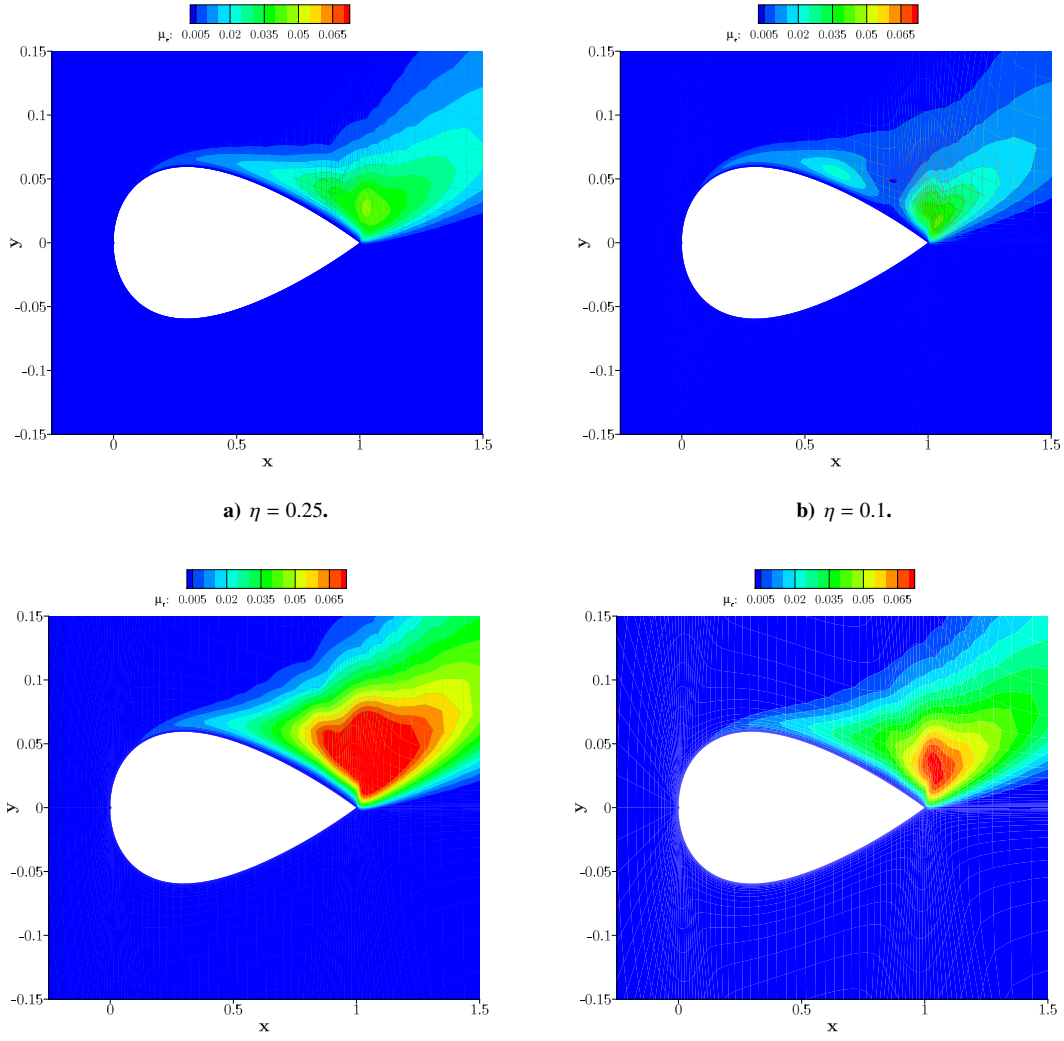

a) $\eta = 0.25$**.** **b)** $\eta = 0.1$**.**

c) $\eta = 0.05$**.** **d)** $\eta = 0.01$**.**

Figure 7. Turbulent viscosity fields for data assimilations with different noise levels in the synthetic measurements.

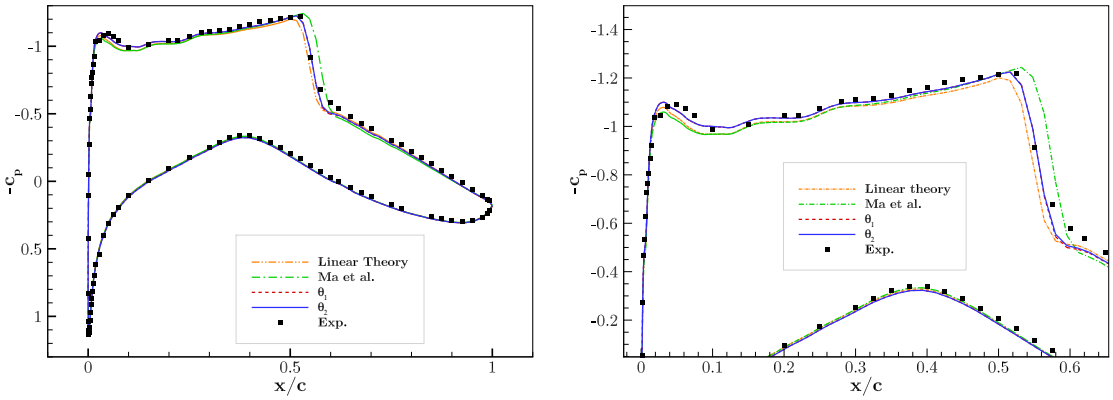

a) c_p **distribution over the airfoil.** **b)** c_p **distribution over the upper surface of the airfoil.**

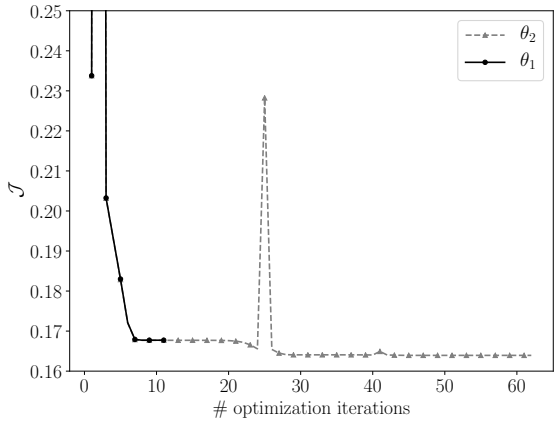

c) Optimization history.

Figure 8. Comparison of results between data assimilations with different parameter spaces.

for this test case. This was expected, since the flow conditions are only weakly non-linear, and the effect of turbulence is limited solely to the boundary layer region. However, Tab. 4 demonstrates that the assimilation with $\boldsymbol{\theta_2}$ better matches the experimentally-measured lift and pitching moment coefficients. Furthermore, the assimilation with $\boldsymbol{\theta_2}$ outperforms both the corrections done using linear theory and the data assimilation of Ma et al. [21]. The results of the latter two approaches were obtained by running simulations in SU2 with the proposed corrected values for α and M, and a fixed $\boldsymbol{\beta}$ value of unity. It is worth noting that the results obtained by using the corrections of Ma et al. yield a higher objective function than that obtained by using the corrections from linear theory. This could be due to a number of reasons, e.g. using different flow solvers and numerical methods, different grids, different objective functions.

Table 4. Comparison of the results of the different data assimilations for case 6.

	$\mathcal{J}$	α [deg]	M	c_L	c_m
Reference	-	2.92	0.725	0.743	−0.095
$\boldsymbol{\theta_1}$	0.1677	2.40	0.730	0.740	−0.093
$\boldsymbol{\theta_2}$	0.1639	2.40	0.730	0.741	−0.094
Ma et al. [21]	0.3850	2.37	0.735	0.737	−0.096
Linear theory	0.2315	2.31	0.729	0.724	−0.093

Next, the stream-wise velocity ratio u/U of the boundary layer was compared with that from the experiments in order to check the results against data that were not used in the assimilation procedure. The following locations on the upper surface of the airfoil were selected for the comparisons: $x/c = 0.179, 0.319, 0.9, 0.95$, the latter two of which are located after the shock. Figures 9a and 9b show that there are no significant differences between the two assimilated results before the shock. This was expected since no complex phenomenon to be simulated by the turbulence model is present on the first part of the airfoil surface. Similarly, the boundary layers of the two assimilated results after the shock are indistinguishable and agree very well with the experimental results. This is shown in Fig. 9c and Fig. 9d.

From these results we can conclude that data assimilation is an effective tool for the corrections of wind tunnel wall interference in the weakly non-linear regime, providing more accurate results than corrections based on linear theory. We observed that using $\boldsymbol{\theta_2}$ instead of $\boldsymbol{\theta_1}$ as vector of control parameters only marginally improves the results of the data assimilation for this case, where no separation after the shock wave is present and the non-linear effects of the flow are confined in a very small region within the boundary layer.

B. RAE 2822 - Case 10

Case 10 presents shock-induced boundary layer separation and, as such, poses a more challenging condition for both classical linear corrections and data assimilation. The initial condition for the data assimilations with vector of control parameters identified by $\boldsymbol{\theta_1}$ and $\boldsymbol{\theta_2}$ corresponded to the values of Mach number and angle of attack suggested by Rudnik [32], i.e. $M = 0.75$, $\alpha = 2.80$ deg. The initial value of $\boldsymbol{\beta}$ was set to unity everywhere in the domain.
Figure 10a shows the optimization history for the two data assimilations. The assimilation with $\boldsymbol{\theta_2}$ reduces the objective function of more than 60 % compared to the initial value, whereas the assimilation with $\boldsymbol{\theta_1}$ attains a minimum when the objective function is reduced by 'only' 50 %. Hence, including $\boldsymbol{\beta}$ in the vector of control parameters helps in improving the assimilation results for this mildly non-linear case.

Figure 10b compares the airfoil c_p distribution of the assimilated results with that of the reference and that of the baseline case, i.e. obtained by running a simulation with the initial conditions specified for the assimilation. The assimilations focus on better resolving the shock location which is largely over-predicted by the baseline results. This, however, slightly decreases the magnitude of the low pressure peak on the upper surface at the leading edge. The assimilation with $\boldsymbol{\theta_2}$ resolves the pressure coefficient distribution after the shock much better than that with $\boldsymbol{\theta_1}$ and the baseline simulation, hence the clear advantage of using the discrepancy term as control parameter.

Table 5 summarizes some of the results for this case. We can observe as the c_L and c_m predicted by the assimilations are much closer to the reference than the baseline results. In particular the c_L and c_m for the assimilation with $\boldsymbol{\theta_2}$ have an error of only 0.8% and 0.9% with respect to the reference. Both assimilations suggest to correct the reference Mach number to a higher one, while opposite corrections are proposed for the angle of attack. While the assimilation with $\boldsymbol{\theta_1}$ proposed a smaller α than in the experiment, the one with $\boldsymbol{\theta_2}$ suggested that increasing the angle of attack would be an appropriate correction. This is due to the effect of the discrepancy term, which significantly changes the flow dynamics and, in turns, affects the optimal values of the other control parameters.

Finally, by looking at the boundary layer comparisons of Fig. 11, one can observe that both the assimilated and the baseline results are capable of correctly reproducing the boundary layer shape before the shock location. On the

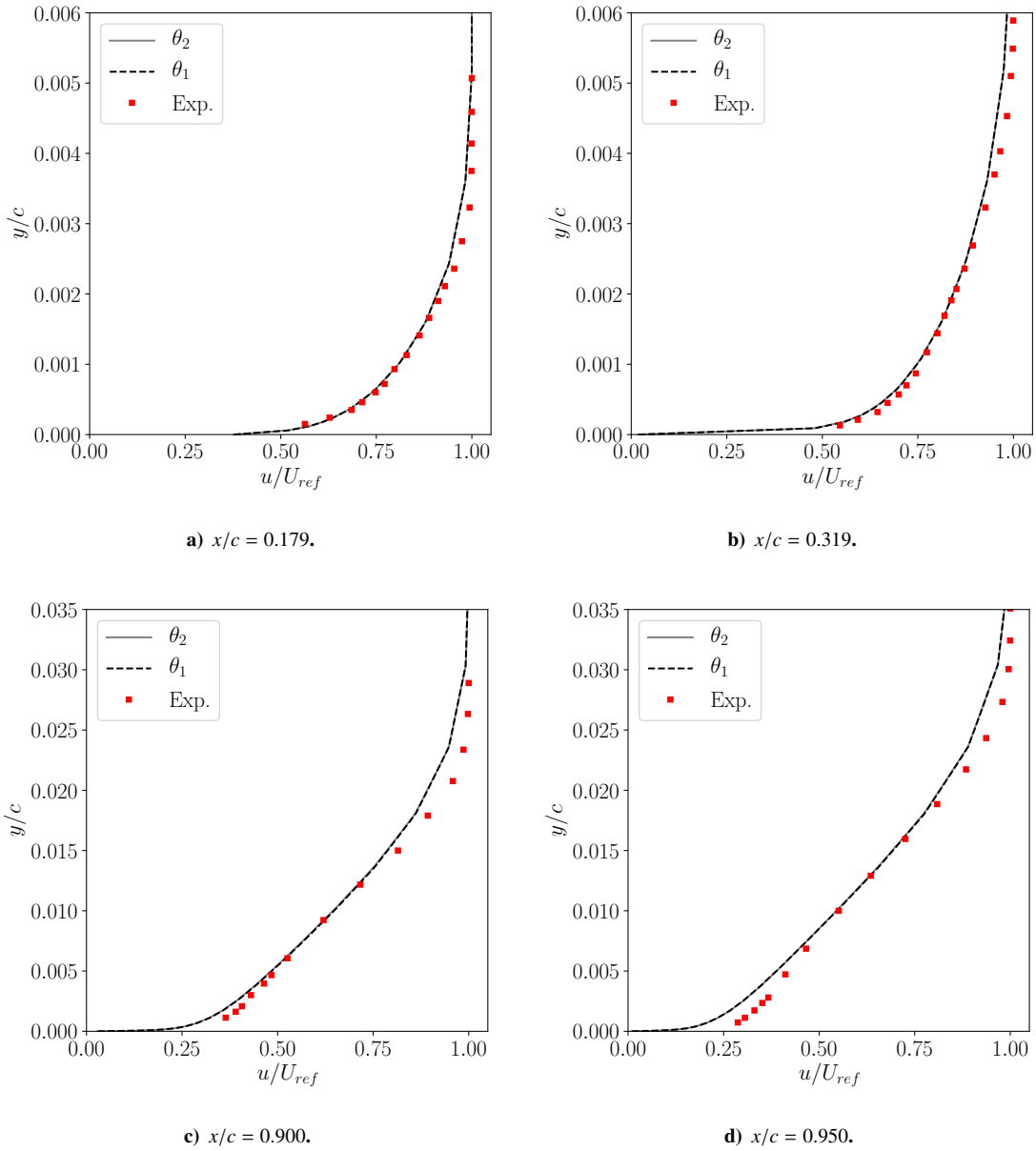

a) $x/c = 0.179$. **b)** $x/c = 0.319$.

c) $x/c = 0.900$. **d)** $x/c = 0.950$.

Figure 9. Comparison of boundary layers at different x/c locations on the upper surface of the airfoil.

Table 5. Comparison of the results of the different data assimilations for case 10.

	$\mathcal{J}$	α [deg]	M	c_L	c_m
Reference	-	3.19	0.75	0.743	−0.106
$\boldsymbol{\theta_1}$	0.6345	3.22	0.764	0.732	−0.102
$\boldsymbol{\theta_2}$	0.5284	3.00	0.760	0.737	−0.105
Baseline	1.3359	2.80	0.750	0.772	−0.098

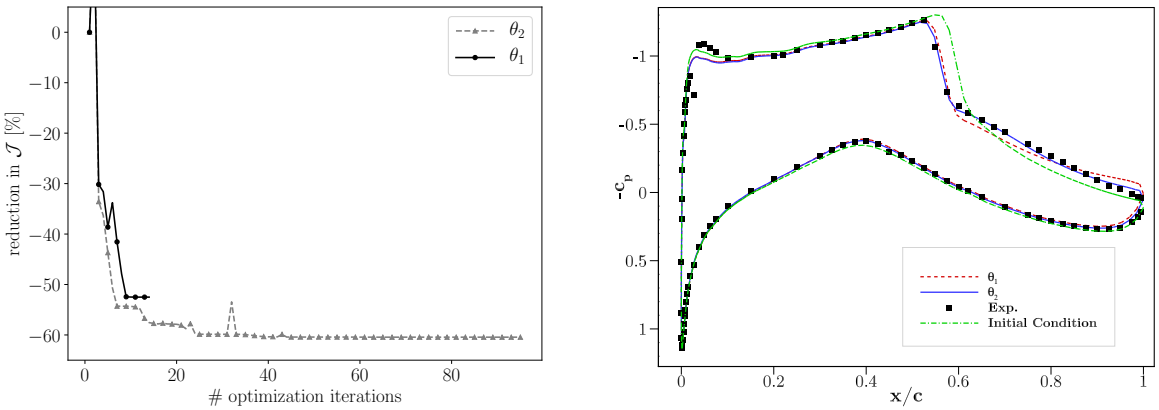

a) Optimization history. **b) c_p distribution over the airfoil.**

Figure 10. Comparison of results between data assimilations with different parameter spaces.

other hand, it appears that the assimilated results better reproduce the flow immediately after the shock at $x/c = 0.75$, whereas the baseline is better close to the trailing edge of the airfoil at $x/c = 0.90$.

All in all, we can conclude that the assimilated results are better than the baseline at reproducing the c_p distribution around the airfoil and, consequently, at matching the lift and pitching moment coefficients of the experiments. They do so by correcting the angle of attack and Mach number to the corresponding free-stream conditions and, in the case of the assimilation with $\boldsymbol{\theta_2}$, by correcting the model form uncertainty in the turbulence model. Despite this, the assimilated results are not capable of reproducing the experimental boundary layer in proximity of the trailing edge of the wing. This could be due to a number of reasons. It is possible that the c_p distribution on the airfoil is not sufficiently informative for the data assimilation to correctly reconstruct the velocity field. It can also be due to the intrinsic inability of linear eddy viscosity turbulence models to reproduce anisotropic turbulent phenomena; if this is the case, inserting $\boldsymbol{\beta}$ within the turbulence transport equation will not be sufficient to match the experimental results. Another possible explanation is that, given the major discrepancies between the experiments and the baseline results (which are based on linear corrections), the experimental results could simply be un-correctable.

V. Conclusions

In this work we assessed the potentials of a variational data assimilation technique for correcting wind tunnel wall interference. The data assimilation minimizes the difference between a quantity of interest measured during the experiment, and the values of the same quantity as obtained from RANS simulations. The control variables utilized are the angle of attack, the Mach number, and a corrective field that takes into account the errors in the mathematical form of the turbulence model.

First, we validated the framework with synthetic data. These were taken to be the pressure coefficient on a NACA 0012 airfoil computed using the SST turbulence model. The turbulence model used for the data assimilations was the SA model. We observed, that when the full, noiseless set of synthetic data is used, the data assimilation perfectly retrieves the correct Mach number, with an error in the angle of attack of only 0.5%. Second, we analyzed the sensitivity of the data assimilation technique to the number of available data and to the level of noise in the measurements. In the first case, we concluded that the assimilation could work even with a very limited number of measurements. Indeed, when only 4% of the original data set was used, the methodology analyzed in this paper could still assimilate the Mach number with no error, and the angle of attack with an error smaller than 1%. In the second case, we observed that the data assimilation was able to keep the error below 5.2% for the angle of attack and below 1.3% for the Mach number even with extremely noisy data. However, the reconstruction of the pressure distribution close to the trailing edge of the airfoil deteriorated with increasing noise level, potentially leading to a mistaken prediction of the force coefficients.

Finally, the methodology was tested on experimental data. Uncorrected measurements from a wind tunnel experiment on the RAE 2822 airfoil were used. Cases 6 and 10 of the database were analyzed, for they present complex flow features complicating the use of simple, linear corrections to the Mach number and angle of attack. The data assimilation was able to reproduce the measured pressure distribution by accurately tuning the angle of attack and

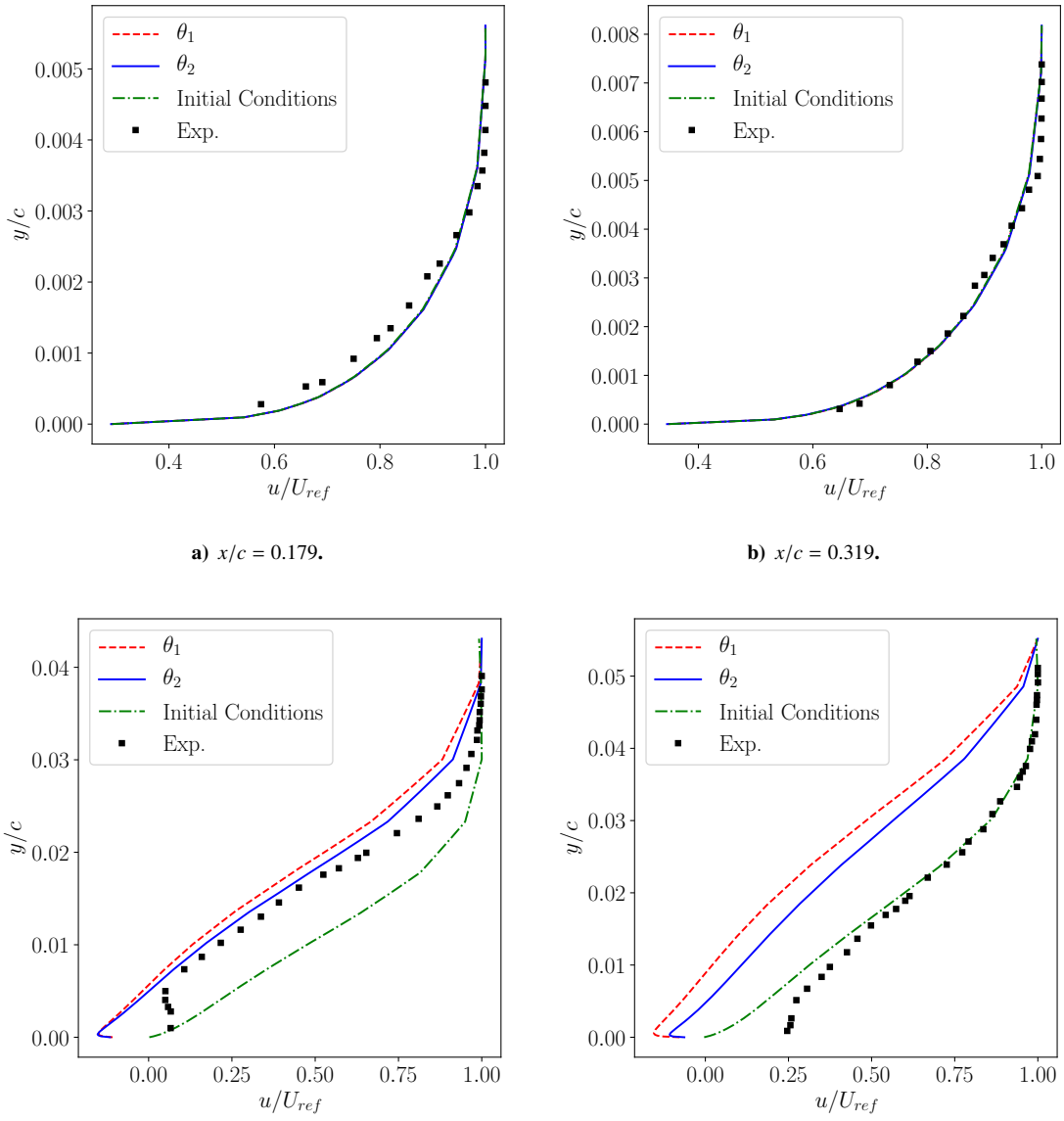

a) $x/c = 0.179$.

b) $x/c = 0.319$.

c) $x/c = 0.750$.

d) $x/c = 0.900$.

Figure 11. Comparison of boundary layers at different x/c locations on the upper surface of the airfoil.

Mach number, and by correcting the errors in the turbulence model. It was shown that using a discrepancy term in the vector of control variables is fundamental if accurate corrections have to be obtained. The methodology presented in this work outperforms both linear correction techniques and data assimilations not taking into account the discrepancy term. However, the possibility that the pressure coefficient on the airfoil does not provide enough information to accurately reconstruct the velocity field was noted and this phenomenon needs to be analyzed further.

In conclusion, the variational data assimilation assessed in this paper proved to be a comprehensive framework for the correction of wind tunnel wall interference. Its ability to work with little data or high noise levels was proven. Further studies should try to assess its capability to correctly reconstruct the velocity field by using only pressure data, and to produce a comprehensive study of the uncertainties in the assimilated results.

References

[1] M. Melanson, M. Chang, and W. Baker II, "Wind tunnel testing's future: A vision of the next generation of wind tunnel test requirements and facilities," in *48th AIAA Aerospace Sciences Meeting Including the New Horizons Forum and Aerospace Exposition*, p. 142, 2010.

[2] F. T. Johnson, E. N. Tinoco, and N. J. Yu, "Thirty years of development and application of cfd at boeing commercial airplanes, seattle," *Computers & Fluids*, vol. 34, no. 10, pp. 1115–1151, 2005.

[3] B. Ewald, "Agardograph 336," *Wind tunnel wall correction*, 1998.

[4] S. C. Dunn, J. R. Micol, D. Myren, and R. W. Paryz, "Gttc future of ground testing meta-analysis of 20 documents," in *2018 AIAA Aerospace Sciences Meeting*, p. 0387, 2018.

[5] M. R. Malik and D. M. Bushnell, "Role of computational fluid dynamics and wind tunnels in aeronautics r and d," 2012.

[6] F.-X. Le Dimet and O. Talagrand, "Variational algorithms for analysis and assimilation of meteorological observations: theoretical aspects," *Tellus A: Dynamic Meteorology and Oceanography*, vol. 38, no. 2, pp. 97–110, 1986.

[7] S. H. Cheung, T. A. Oliver, E. E. Prudencio, S. Prudhomme, and R. D. Moser, "Bayesian uncertainty analysis with applications to turbulence modeling," *Reliability Engineering & System Safety*, vol. 96, no. 9, pp. 1137–1149, 2011.

[8] W. Edeling, P. Cinnella, R. P. Dwight, and H. Bijl, "Bayesian estimates of parameter variability in the k–ε turbulence model," *Journal of Computational Physics*, vol. 258, pp. 73–94, 2014.

[9] W. Edeling, P. Cinnella, and R. P. Dwight, "Predictive rans simulations via bayesian model-scenario averaging," *Journal of Computational Physics*, vol. 275, pp. 65–91, 2014.

[10] K. Duraisamy, Z. J. Zhang, and A. P. Singh, "New approaches in turbulence and transition modeling using data-driven techniques," in *53rd AIAA Aerospace Sciences Meeting*, p. 1284, 2015.

[11] E. J. Parish and K. Duraisamy, "A paradigm for data-driven predictive modeling using field inversion and machine learning," *Journal of Computational Physics*, vol. 305, pp. 758–774, 2016.

[12] A. P. Singh and K. Duraisamy, "Using field inversion to quantify functional errors in turbulence closures," *Physics of Fluids*, vol. 28, no. 4, p. 045110, 2016.

[13] A. P. Singh, K. Duraisamy, and Z. J. Zhang, "Augmentation of turbulence models using field inversion and machine learning," in *55th AIAA Aerospace Sciences Meeting*, p. 0993, 2017.

[14] E. Dow and Q. Wang, "Quantification of structural uncertainties in the k-w turbulence model," in *52nd AIAA/ASME/ASCE/AHS/ASC Structures, Structural Dynamics and Materials Conference 19th AIAA/ASME/AHS Adaptive Structures Conference 13t*, p. 1762, 2011.

[15] E. Dow and Q. Wang, "Uncertainty quantification of structural uncertainties in rans simulations of complex flows," in *20th AIAA Computational Fluid Dynamics Conference*, p. 3865, 2011.

[16] M. E. Hayek, Q. Wang, and G. M. Laskowski, "Adjoint-based optimization of rans eddy viscosity model for u-bend channel flow," in *2018 AIAA Aerospace Sciences Meeting*, p. 2091, 2018.

[17] D. P. Foures, N. Dovetta, D. Sipp, and P. J. Schmid, "A data-assimilation method for reynolds-averaged navier–stokes-driven mean flow reconstruction," *Journal of Fluid Mechanics*, vol. 759, pp. 404–431, 2014.

[18] S. Symon, N. Dovetta, B. J. McKeon, D. Sipp, and P. J. Schmid, "Data assimilation of mean velocity from 2d piv measurements of flow over an idealized airfoil," *Experiments in fluids*, vol. 58, no. 5, p. 61, 2017.

[19] M. Lemke and J. Sesterhenn, "Adjoint-based pressure determination from piv data in compressible flowsvalidation and assessment based on synthetic data," *European Journal of Mechanics-B/Fluids*, vol. 58, pp. 29–38, 2016.

[20] V. Mons, J.-C. Chassaing, T. Gomez, and P. Sagaut, "Reconstruction of unsteady viscous flows using data assimilation schemes," *Journal of Computational Physics*, vol. 316, pp. 255–280, 2016.

[21] B. Ma, G. Wang, Z. Ye, and L. Xu, "A numerical method for transonic wind tunnel wall interference correction in airfoil testing," in *34th AIAA Applied Aerodynamics Conference*, p. 3575, 2016.

[22] H. Kato, A. Yoshizawa, G. Ueno, and S. Obayashi, "A data assimilation methodology for reconstructing turbulent flows around aircraft," *Journal of Computational Physics*, vol. 283, pp. 559–581, 2015.

[23] F. Palacios, J. Alonso, K. Duraisamy, M. Colonno, J. Hicken, A. Aranake, A. Campos, S. Copeland, T. Economon, A. Lonkar, *et al.*, "Stanford university unstructured (su 2): an open-source integrated computational environment for multi-physics simulation and design," in *51st AIAA Aerospace Sciences Meeting including the New Horizons Forum and Aerospace Exposition*, p. 287, 2013.

[24] F. Palacios, T. D. Economon, A. Aranake, S. R. Copeland, A. K. Lonkar, T. W. Lukaczyk, D. E. Manosalvas, K. R. Naik, S. Padron, B. Tracey, *et al.*, "Stanford university unstructured (su2): Analysis and design technology for turbulent flows," in *52nd Aerospace Sciences Meeting*, p. 0243, 2014.

[25] D. C. Wilcox *et al.*, *Turbulence modeling for CFD*, vol. 2. DCW industries La Canada, CA, 1998.

[26] F. M. White and I. Corfield, *Viscous fluid flow*, vol. 3. McGraw-Hill New York, 2006.

[27] P. Spalart and S. Allmaras, "A one-equation turbulence model for aerodynamic flows," in *30th aerospace sciences meeting and exhibit*, p. 439, 1992.

[28] T. A. Albring, M. Sagebaum, and N. R. Gauger, "Development of a consistent discrete adjoint solver in an evolving aerodynamic design framework," in *16th AIAA/ISSMO Multidisciplinary Analysis and Optimization Conference*, p. 3240, 2015.

[29] T. A. Albring, M. Sagebaum, and N. R. Gauger, "Efficient aerodynamic design using the discrete adjoint method in su2," in *17th AIAA/ISSMO multidisciplinary analysis and optimization conference*, p. 3518, 2016.

[30] F. R. Menter, "Two-equation eddy-viscosity turbulence models for engineering applications," *AIAA journal*, vol. 32, no. 8, pp. 1598–1605, 1994.

[31] P. Cook, M. Firmin, and M. McDonald, *Aerofoil RAE 2822: pressure distributions, and boundary layer and wake measurements*. RAE, 1977.

[32] R. Rudnik, "Untersuchung der leistungsfähigkeit von zweigleichungs-turbulenzmodellen bei profilumströmungen," *FORSCHUNGSBERICHT-DEUTSCHES ZENTRUM FUR LUFT UND RAUMFAHRT*, 1997.